HHS Public Access

Author manuscript

FASEB J. Author manuscript; available in PMC 2023 January 01.

Published in final edited form as:

FASEB J. 2022 January ; 36(1): e22106. doi:10.1096/fj.202101085RR.

Selectively Targeting Disease-Restricted Secretogranin III to Alleviate Choroidal Neovascularization

Liyang Ji[1,2,3,*], **Prabuddha Waduge**[1,2,*], **Lili Hao**[2,4], **Avinash Kaur**[1,2], **Wencui Wan**[2,5], **Yan Wu**[2], **Hong Tian**[6], **Jinsong Zhang**[3], **Keith A. Webster**[1,2,6], **Wei Li**[1,2]

[1]Cullen Eye Institute, Department of Ophthalmology, Baylor College of Medicine, Houston, TX.

[2]Bascom Palmer Eye Institute, University of Miami School of Medicine, Miami, FL.

[3]Department of Ophthalmology, The Fourth Affiliated Hospital of China Medical University, Shenyang, Liaoning, China.

[4]Department of Ophthalmology, The First Affiliated Hospital of Jinan University, Guangzhou, Guangdong, China

[5]Department of Ophthalmology, The First Affiliated Hospital of Zhengzhou University, Zhengzhou, Henan, China

[6]Everglades Biopharma, LLC, Houston, TX

Abstract

Choroidal neovascularization (CNV), a leading cause of blindness in the elderly, is routinely treated with vascular endothelial growth factor (VEGF) inhibitors that have limited efficacy and potentially adverse side effects. An unmet clinical need is to develop novel therapies against other angiogenic factors for alternative or combination treatment to improve efficacy and safety. We recently described secretogranin III (Scg3) as a disease-selective angiogenic factor, causally linked to diabetic retinopathy and acting independently of the VEGF pathway. An important question is whether such a disease-selective Scg3 pathway contributes to other states of pathological angiogenesis beyond diabetic retinopathy. By applying a novel *in vivo* endothelial ligand binding assay, we found that the binding of Scg3 to CNV vessels in live mice was markedly increased over background binding to healthy choriocapillaris and blocked by an Scg3-neutralizing antibody, whereas VEGF showed no such differential binding. Intravitreal injection of anti-Scg3 humanized antibody Fab (hFab) inhibited Matrigel-induced CNV with similar efficacy to the anti-VEGF drug aflibercept. Importantly, a combination of anti-Scg3 hFab and aflibercept synergistically alleviated CNV. Homozygous deletion of the Scg3 gene markedly reduced CNV severity and abolished the therapeutic activity of anti-Scg3 hFab, but not aflibercept, suggesting a role for Scg3 in

Correspondence: Wei Li, Cullen Eye Institute, Department of Ophthalmology, Baylor College of Medicine. Address: One Baylor Plaza, NC205, Houston, TX 77030, USA. Tel: 713-798-8885; Fax: 713-798-3026, wei.li4@bcm.edu.

*LJ and PW contributed equally to this paper.

AUTHOR CONTRIBUTIONS

LJ, PW, LH, AK and WW performed experiments and analyzed data. YW, JZ and KAW provided technical support. HT provided key resources. WL conceptualized and supervised the study. LJ, WL and KAW wrote the manuscript. All authors approved the final version of the manuscript.

Conflict of interest: HT and WL are shareholders of Everglades Biopharma, LLC and LigandomicsRx, LLC. WL is an inventor of issued and pending patents. The remaining authors declare no competing financial interests.

VEGF-independent CNV pathogenesis and therapy. Our work demonstrates the stringent disease selectivity of Scg3 binding and positions anti-Scg3 hFab as a next-generation disease-targeted anti-angiogenic therapy for CNV.

Keywords

Secretogranin III; angiogenic factor; anti-angiogenic therapy; choroidal neovascularization; age-related macular degeneration

1. INTRODUCTION

Neovascular or wet age-related macular degeneration (AMD) caused by choroidal neovascularization (CNV) is a leading cause of vision impairment among the elderly in developed countries (1). Approval of anti-angiogenic drugs against vascular endothelial growth factor (VEGF) to alleviate CNV constituted a major breakthrough in AMD therapy (2, 3). However, despite the efficacy improvements over traditional photodynamic therapy, more than half of patients respond poorly with minimal or no improvement in visual acuity, and long-term outcomes even among responders are suboptimal (4-6). Efforts to complement anti-VEGF by targeting alternative signaling molecules, including platelet-derived growth factor and angiopoietin-2, have so far been unsuccessful (7). Despite the clinical use of multiple anti-VEGF drugs, including ranibizumab, aflibercept, bevacizumab, pegaptanib, brolucizumab and conbercept, VEGF continues to represent the key target for the majority of ongoing clinical trials (7), a phenomenon that highlights the unmet need to identify VEGF-independent targets to complement or replace anti-VEGF therapies (8, 9).

Our group has reported that secretogranin III (Scg3) binds to endothelia and drives pathological neovascularization and vascular leakage selectively in diabetic but not healthy mice (10, 11). This is in contrast to VEGF that binds to multiple target cells and promotes angiogenesis and vascular leakage indiscriminately in both diseased and healthy vasculatures (10-12). Scg3-neutralizing monoclonal antibodies (mAbs) alleviate pathological angiogenesis and vascular leakage in various mouse models of ocular diseases, including laser- or Matrigel-induced CNV, with optimal safety (10, 13, 14). However, disease selectivity of Scg3 as it relates to CNV has not been characterized.

Here, by implementing a novel ligand binding assay, we quantified and compared the binding specificities of Scg3 and VEGF to relevant cell types *in vitro* and to CNV and healthy choriocapillaris *in vivo*. We created a humanized anti-Scg3 Fab fragment (hFab) and characterized its therapeutic activity in a Matrigel-induced CNV (MCNV) model of wet AMD. Interestingly, a combination of anti-Scg3 and anti-VEGF synergistically ameliorated MCNV. Our results indicate highly stringent disease-selective binding of Scg3 and high efficacy of anti-Scg3 hFab to block CNV in this model. The findings support our contention that anti-Scg3 hFab represents a unique ligand-guided disease-targeted anti-angiogenic therapy for wet AMD that is safe and highly efficacious.

2. MATERIALS AND METHODS

2.1. Animals and materials

C57BL/6J and Scg3-knockout mice (6-8 weeks old, male or female) were purchased from the Jackson Laboratory and Taconic Bioscience (Model #TF3191), respectively. Scg3-knockout mice were backcrossed to C57BL/6J for at least five generations. $Scg3^{-/-}$ mice were verified by genotyping and quantification of mRNA and protein expression in the retina and brain by reverse transcription PCR and Western blot (15). All animal procedures were approved by the Institutional Animal Care and Use Committee at the University of Miami and Baylor College of Medicine. Human umbilical vein endothelial cells (HUVECs), human adult retinal pigment epithelial (RPE)-19 (ARPE19) cell line and mouse Neuro-2a cell line were previously described (10, 16).

2.2. Anti-Scg3 humanized antibody (hAb)

Anti-Scg3 hAb and related hFab (Clone EBP2) were generated from Scg3-neutralizing ML49.3 mAb (10) by Everglades Biopharma, LLC (Houston, TX). Binding kinetics measurements were implemented using an Octet QKe system (ForteBio, Fremont, CA), as described (17). Briefly, human Scg3 (hScg3) was labeled with biotin using NHS-PEG4-Biotin (Thermo Fisher Scientific, Waltham, MA, Cat #A39259), followed by desalting purification. Biotin-Scg3 was loaded on to streptavidin biosensors in the Octet instrument, washed and bound to purified anti-Scg3 ML49.3 mAb, full-length hAb or hFab. Antibody binding affinities were calculated using the Octet software. Epitope binning was performed to analyze the binding competition between ML49.3 mAb and the hFab using the Octet. Briefly, streptavidin biosensors bound to biotinylated hScg3 or mouse Scg3 (mScg3) were incubated with anti-Scg3 hFab, followed by washing and binding of ML49.3 mAb, non-neutralizing control ML190.2 mAb (10) or no-competing ML78.2 mAb (14) to study the competition between antibodies (Abs). Additionally, hScg3 or mScg3 was immobilized on ELISA plates, blocked and incubated with different anti-Scg3 Abs. Bound Abs were detected with horseradish peroxidase-conjugated anti-mouse IgG or anti-human IgG secondary Abs, followed by colorimetric assay.

2.3. MCNV

MCNV was induced in both eyes of mice, as described (18). Briefly, growth factor-reduced Matrigel (Corning, Corning, NY, Cat. #354263) was diluted 3:1 with PBS and injected into the subretinal space of anesthetized mice (1 μl/eye) to induce CNV on Day 0.

2.4. *In vitro* endothelial functional assays.

Endothelial proliferation was performed as described (10, 19). Briefly, Scg3 or VEGF was incubated with HUVECs in the presence or absence of anti-Scg3 hFab or aflibercept (Regeneron Pharmaceuticals, Tarrytown, NY), respectively, and added to HUVECs in 96-well plates or 24-well transwell plates. Endothelial cells were quantified for cell proliferation at 48 h in 96-well plates or for transwell migration at 20 h in 24-well plates.

2.5. Construction and characterization of Scg3-Phage

Clonal T7 phage displaying full-length hScg3 (Scg3-Phage) was constructed as described (10, 20). Briefly, the Scg3 coding region with optimized codons was synthesized and cloned into an improved T7Bio3C phage display vector (20) to generate Scg3-Phage. Clonal phage displaying $VEGF_{110}$ (VEGF-Phage) was previously reported (10). Scg3-Phage and VEGF-Phage were analyzed for binding by ELISA. Briefly, anti-Scg3 hFab, aflibercept (Regeneron Pharmaceutical), control hFab (Sigma, St. Louis, MO) or BSA was immobilized on ELISA plates (0.1 μg/well), washed, blocked and preincubated with or without hScg3, mScg3, VEGF (1 μg/ml) or mock buffer. Fresh lysate of Scg3-Phage or VEGF-Phage was added to each well (~5 x 10^{10} pfu/ml) and incubated for 1 h at room temperature in the presence of 0.5% Tween-20. After washing, bound phages were eluted with PBS containing 0.5% SDS and quantified by phage plaque assays (20).

2.6. *In vitro* and *in vivo* ligand binding assays

For *in vitro* cell-based ligand binding assays, Scg3-Phage and VEGF-Phage were amplified in BLT5615 bacteria, precipitated, purified by CsCl gradient centrifugation, dialyzed against PBS and titrated by phage plaque assay. Purified phages were pretreated with human rhinovirus (HRV) 3C protease (ACROBiosystems) (100 units/ml) or PBS control overnight at 4°C to remove Scg3 or VEGF from the phage surface (20). Phages were preincubated with anti-Scg3 hFab, aflibercept (4 μg/ml) or PBS for 30 min at 4°C and added to HUVECs, ARPE-19 or Neuro-2a cells in 48-well plates (1 x 10^{12} pfu/well). After incubation at 37°C for 30 min in the presence of 1% BSA, cells were washed three times with PBS containing 1% BSA within 3 min and lysed with PBS containing 0.5% SDS. Cell-bound phages were quantified by plaque assay.

In vivo endothelium-binding assays were performed, as described previously with modifications (10). Briefly, purified Scg3-Phage and VEGF-Phage were pretreated with or without HRV 3C protease as above, incubated with anti-Scg3 hFab, aflibercept (4 μg/ml) or PBS at 4°C for 30 min and injected i.v. into anesthetized mice with MCNV at Day 7 (1 x 10^{12} pfu/mouse). After circulating for 20 min, mice were euthanized by CO_2 inhalation, immediately followed by intracardial perfusion with 70 ml PBS for 7 min to remove unbound phages. After removal of the anterior section and neural retina from enucleated eyes, paired tissues of similar size with or without CNV lesion were isolated from RPE-choroid-sclera complexes (RPE eyecups) of the same eye, weighed and homogenized in PBS with 1% Triton X-100 until no solid tissues were visible. Vessel-bound phages in homogenates were quantified by plaque assays.

2.7. Therapy of MCNV

Anti-Scg3 hFab, control human IgG Fab, aflibercept (1 μl/eye) or PBS was injected intravitreally 3 days post MCNV induction. Both eyes of each mouse randomly received different therapeutic agents. To avoid bias, reagents were blind-coded. Therapeutic efficacy was analyzed for CNV leakage at Day 7 using fluorescein angiography (FA) in anesthetized mice. After euthanasia, RPE eyecups were prepared for choroidal immunostaining with Alexa Fluor 488-conjugated isolectin B4 (AF488-IB4) to label CNV and analyzed as described below.

2.8. FA

FA was performed as described (13, 21). Briefly, fluorescein sodium (0.1 ml, 2.5%) was injected i.p. into anesthetized mice. FA images were captured 6 min post injection using a Heidelberg Engineering Multiline HRA SN 2884 imaging system. Instrument settings for detection sensitivity were standardized. CNV leakage intensity and leakage area were quantified using ImageJ software (NIH). All captures were normalized against the total intensity of the entire retinal field.

2.9. Choroidal immunostaining

After FA capture, mice were allowed 6 h to eliminate fluorescein sodium through urination. Eyes were enucleated from euthanized mice and fixed with 1% paraformaldehyde for 40 min at room temperature. RPE eyecups were isolated, permeabilized with 0.5% Triton X-100 in PBS for 2 h and stained with AF488-IB4 (10 μg/ml) overnight to label CNV vessels (13, 21). After washing, RPE eyecups were flat mounted, analyzed using a Keyence BZ-X810 structured illumination microscope (SIM) and quantified for CNV 3D volume and maximal lesion area using the Keyence software.

2.10. H&E staining and immunohistochemistry

Eyes were enucleated from euthanized mice at Day 7 after CNV induction and fixed in Davidson solution (22) for hematoxylin and eosin (H&E) staining or 4% paraformaldehyde for immunohistochemistry and embedded in optimal cutting temperature compound (OCTC). Cryosections of eyes at 6-μm thickness were stained with H&E and analyzed using the SIM microscope. Additionally, tissue sections were stained with anti-Scg3 rabbit polyclonal Abs (10) and anti-CD31 mouse mAb (Abcam, #ab24590), followed by Alexa Fluor 594 anti-rabbit IgG F(ab')2 and AF488-anti-mouse Ab and analyzed using the SIM.

To visualize *in vivo* ligand binding, Scg3-Phage was amplified in BLT7FLAG *E. coli* (20), purified by CsCl gradient centrifugation, dialyzed against PBS, titrated and used for *in vivo* binding in MCNV mice as described above. At the end of binding, mice were intracardially perfused with PBS, followed by 4% paraformaldehyde. Eyes were enucleated, refixed, embedded in OCTC, sectioned at 5-μm thickness and probed with rabbit anti-FLAG polyclonal Abs, followed by Alexa Fluor 594 anti-rabbit IgG F(ab')2 and AF488-IB4. After washing, fluorescent signals were detected, as described above.

2.11. Optical coherence tomography (OCT)

Mice were anesthetized, and pupils were dilated with phenylephrine eyedrops. Retinas were scanned by a Heidelberg Engineering Spectral Domain OCT (SD-OCT), as described (23).

2.12. Western blot

After intravitreal injection of anti-Scg3 hFab, aflibercept or control hFab on Day 3 post CNV induction, eyes were enucleated at Day 7. MCNV and healthy choroid of equal size were isolated from the same RPE eyecups, weighed, homogenized in RIPA buffer (Thermo Fisher), quantified for proteins and analyzed by Western blot using Abs against ERK,

phosphorylated ERK (p-ERK), Src, p-Src and β-actin (10). Western blots of Scg3 were performed, as previously described (10).

2.13. Statistics

Data are expressed as mean ± SEM. Intergroup differences were analyzed using one-way ANOVA or Student's t-test.

3. RESULTS

3.1. Characterization of an MCNV disease model

To characterize the contributions of Scg3 to pathological angiogenesis in a model of wet AMD, we first delineated the time course of MCNV in mice injected with subretinal Matrigel. FA revealed that CNV leakage was detectable at Day 5 and markedly intensified at Day 7 (Figure 1A; top panel). CNV leakage peaked at Day 14 and remained robust at Day 21. At Day 30, the area of CNV leakage remained extensive but with decreased intensity. The trend continued through Day 40.

To independently verify the disease time course, RPE eyecups were isolated at the same time points, and CNV vessels were stained with AF488-IB4. Fluorescence analyses of stained vessels confirmed CNV at Day 5 with rapid expansion through Days 7 and 14 (Figure 1A; middle and bottom panels). Neovessel area and densities associated with CNV were markedly reduced at Days 30 and 40. Representative 3D images of the CNV vasculature, including top, intermediate, deep and bottom vessels, are shown in Figure 1B,C.

To investigate MCNV morphology, we performed histological examinations by H&E staining. Matrigel deposits were clearly visible at Day 7 (Figure 1D), and the entire retina above the Matrigel displayed severe deformation. *In vivo* OCT imaging revealed the presence of subretinal RPE Matrigel with abnormal accumulation of hyper-reflective materials in the subretinal space and retinal detachment at Day 7 (Figure 1E).

Immunohistochemistry revealed that Scg3 is predominantly expressed in the retinal ganglion cells (RGCs), inner plexiform layer (IPL), outer plexiform layer (OPL) and photoreceptor inner segments (Figure 1F). Scg3 expression was markedly reduced in the inner nuclear layer (INL) and outer nuclear layer (ONL) and scarcely detected in the photoreceptor outer segments (Figure 1F). This expression pattern is consistent with previous findings that Scg3 is expressed primarily in secretory and neurotransmitter vesicles (10, 15, 24, 25). Interestingly, strong signals of the endothelial marker, CD31, were detected inside the Matrigel, indicating MCNV-induced vascular extension into the Matrigel (Figure 1F; bottom panel), similar to *in vivo* Matrigel plugs (26). However, overlap between Scg3 and CD31 signals was minimal, confirming low to absent expression of Scg3 in endothelial cells and suggesting a paracrine regulation of angiogenesis by Scg3, perhaps through neurovascular signaling (27). By contrast, VEGF expression increases during CNV (28).

3.2. Scg3 selectively binds to CNV vasculature

Pathological angiogenesis associated with CNV can be driven by increased levels of angiogenic ligands, upregulation of their cognate receptors or both (12). Because an Scg3

receptor (Scg3R) has not yet been identified, its apparent presence or abundance can be only inferred by comparative binding studies. Therefore, to quantify Scg3 binding during CNV, we adapted our published protocol of *in vivo* comparative ligandomics in mouse retina to create a novel ligand binding assay applicable to mouse CNV (10). To do so, we constructed clonal T7 bacteriophage displaying Scg3 (Scg3-Phage) or VEGF (VEGF-Phage) and confirmed that their binding to anti-Scg3 hFab or aflibercept were effectively blocked by excess cognate recombinant Scg3 or VEGF protein, respectively (Figure 2A and B). These data suggest that both ligands are displayed on the T7 phage surface with binding motifs similar to those of their native proteins.

To quantify *in vivo* binding, purified Scg3-Phage and VEGF-Phage were injected i.v. into mice at Day 7 of MCNV for 20-min circulation and binding, followed by intracardial perfusion of PBS to remove unbound phages, as described (10). Choroidal tissues were isolated from euthanized mice, dissected and separated into presence or absence of CNV. After processing as described in Methods, vessel-bound phages were quantified by plaque assays (Figure 2C). Parallel assays using control empty vector phage without displaying any foreign protein were analyzed to eliminate the possibility of artifacts caused by differential phage leakage of CNV versus normal vessels. The results indicate that such leakage during the binding assay was insignificant, thereby validating the binding assay (Figure 2D).

We found that the binding of Scg3-Phage to CNV vessels was increased by 6.0-fold relative to control choriocapillaris 7 days post CNV induction (Figure 2E). The increased binding was blocked by preincubation of Scg3-Phage with an Scg3-neutralizing hFab or HRV 3C protease (Figure 2E) (20). As a control, no Scg3-Phage binding to the choroid was detected in mice 1 h post Matrigel injection, a stage when no CNV was present (Figure 2F). In contrast, VEGF-Phage binding to CNV and healthy choriocapillaris was similar and was minimally blocked by excess aflibercept or 3C protease digestion (Figure 2G). Together, the results suggest that Scg3, but not VEGF, is a CNV-restricted angiogenic factor with markedly increased binding to CNV vessels (Figure 2E,G), whereas Scg3 ligand itself is minimally induced (Figure 1F). The distinctive binding activity patterns of Scg3 versus VEGF in MCNV are similar to those previously reported by our group in mice with diabetic retinopathy (DR) (10).

We further eliminated the possibility of Scg3-Phage leakage by combining *in vivo* ligand binding with conventional immunohistochemistry to visualize vessel-bound Scg3-Phage. To improve detection sensitivity, each phage particle was labeled with more than 400 copies of FLAG tag (see Methods) (20). The results showed that FLAG signals of Scg3-Phage (red fluorescence), but not VEGF-Phage, predominantly overlapped with CNV vessels (green signals) (Figures 2H and S1). No Scg3-Phage signals were detected in healthy choroidal or retinal vessels. As a control, Scg3-Phage failed to bind the choroid at 1 h post MCNV induction, a time point when CNV is not yet present (Figure S2B). Furthermore, intravitreally injected Scg3-Phage failed to bind MCNV at Day 7 post CNV induction (Figure S2A, top panel). These findings confirm that Scg3-Phage selectively binds to MCNV vessels, but not healthy vasculatures, with minimal leakage.

3.3. Scg3-neutralizing hFab

To facilitate the clinical translation of anti-Scg3 to treat CNV and related conditions, we converted our recently reported anti-Scg3 ML49.3 mAb (10) into full-length hAb and hFab. Kinetic analyses using an Octet instrument determined binding affinities (K_D) of 35 nM for ML49.3 mAb, 11 nM for EBP2 hAb and 8.7 nM for hFab (Figure 3A-C). These results indicate that anti-Scg3 hAb and hFab have comparable binding affinities to the parent anti-Scg3 ML49.3 mAb. Epitope binning analyses by Octet revealed that the hAb and hFab competitively bound to the same site on Scg3 as the original ML49.3 mAb, whereas competition by anti-Scg3 ML190.2 or ML78.2 mAbs, included as negative controls, was not observed (Figure 3D,E). Anti-Scg3 mAb and hFab binding to both human and mouse Scg3 was verified by Octet and ELISA analyses (Figure 3D-F). Analyses of the degree of humanness revealed that the Z-scores for the light and heavy chain of anti-Scg3 hFab are 0.419 and 0.666, respectively, which are markedly improved over the Z-scores of −1.124 and −0.941 for the ML49.3 mAb (29).

The neutralizing activity of anti-Scg3 hFab was independently characterized by two functional assays in cultured HUVECs. The results show that Scg3-induced endothelial proliferation was inhibited by anti-Scg3 hFab (Figure 4A). Additionally, anti-Scg3 hFab significantly blocked Scg3-induced migration of HUVECs in trans-well assays (Figure 4B-D). As a positive control, VEGF stimulated proliferation and migration of HUVECs that were blocked by aflibercept. These findings suggest that the neutralizing activity of anti-Scg3 hFab is similar to that of the previously characterized ML49.3 mAb (10, 13, 14).

3.4. Anti-Scg3 hFab alleviates MCNV

Previously we reported that subcutaneous injection of ML49.3 mAb alleviated MCNV with high efficacy (13). Here we investigated the therapeutic efficacy of anti-Scg3 hFab delivered via intravitreal injection before CNV reached its peak of robust pathological neovascularization. Anti-Scg3 hFab (2 μg/eye) injected at Day 3 significantly alleviated the intensity and area size of CNV leakage as quantified by FA at Day 7 (Figure 5A-C). CNV vessel staining and analysis of isolated RPE eyecups revealed that anti-Scg3 hFab markedly reduced the maximal lesion area and 3D volume of the CNV lesion (Figure 5D-F). As a positive control, aflibercept (2 μg/eye) injected intravitreally also ameliorated CNV effectively in terms of vascular leakage and vessel staining (Figure 5A-F). No therapeutic activity was detected for control hFab.

3.5. Dose-response of anti-Scg3 hFab

To determine dose-dependent therapeutic activities, we compared the efficacy of anti-Scg3 hFab, aflibercept and control hFab to inhibit MCNV at 2, 0.5 and 0.1 μg/eye. In addition to the above-described efficacy of 2 μg/eye, anti-Scg3 hFab at 0.5 μg/eye significantly reduced the intensity and area of CNV leakage as well as the maximal lesion area and 3D volume of CNV vessel staining (Figures 5G-J and S3). Aflibercept at 0.5 μg/eye effectively inhibited CNV leakage but not CNV vessel staining. Additionally, at 0.5 μg/eye dosage, anti-Scg3 hFab reduced 3D volume and maximal CNV lesion size to a greater extent than the same dose of aflibercept. At a dose of 0.1 μg/eye, anti-Scg3 hFab and aflibercept inhibited only CNV leakage intensity with no effect on other parameters (Figures 5G-J and S4).

Overall, the dose-response curves revealed similar efficacy of both agents at 2 μg/eye, and a slightly more potent action of anti-Scg3 hFab at 0.5 μg/eye compared with the same dose of aflibercept (Figure 5).

We previously reported that Scg3 activates ERK and Src kinases in HUVECs (10). Western blot analyses confirmed that the phosphorylation of ERK and Src was also significantly increased in the MCNV model (Figure 6A-C). Both anti-Scg3 hAb and aflibercept (2 μg/eye) inhibited MCNV-induced activation of ERK and Src (Figure 6D-F).

3.6. Synergistic combination therapy of anti-Scg3 and anti-VEGF

We previously reported that Scg3 and VEGF have distinct receptor signaling pathways (10) that may support synergism between the respective antibodies to inhibit neovascular disease. Such a synergism would also be consistent with their distinctive receptor binding activities of the two ligands in healthy versus CNV (Figure 2). Indeed, compared to monotherapy with either anti-Scg3 hFab or aflibercept (0.2 μg/eye), the combination (0.1 + 0.1 μg per eye) synergistically and significantly ameliorated MCNV in terms of both CNV leakage and vessel staining ($p<0.05$, 0.01 or 0.001, versus monotherapies, Figure 7).

3.7. Severity of CNV and efficacy of anti-Scg3 hFab in Scg3-null mice

To further corroborate the role of Scg3 in CNV pathogenesis, we compared CNV severity in $Scg3^{-/-}$ versus $Scg3^{+/+}$ mice. We found no evidence of ophthalmic abnormality in Scg3-null mice as determined by fundoscopy, FA, histological examination and immunostaining of the retinal and choroidal vasculatures (Figures S5 and S6) and confirmed the previously reported normal gross phenotype of $Scg3^{-/-}$ mice (30). Subretinal injection of Matrigel resulted in significant reductions of CNV leakage intensity and area as well as CNV 3D volume and maximal lesion area in $Scg3^{-/-}$ vs. $Scg3^{+/+}$ mice (Figure 8A-F), consistent with a significant contribution of Scg3 to MCNV pathogenesis.

To independently verify that anti-Scg3 hFab alleviates MCNV by inhibiting Scg3 instead of other off-targets, we compared the efficacy of anti-Scg3 hFab and aflibercept in Scg3-deficient mice, following induction of CNV. As expected, we found that anti-Scg3 hFab had no detectable therapeutic activity in $Scg3^{-/-}$ mice, whereas aflibercept significantly inhibited MCNV with similar efficacy to wild-type mice (Figure 8G-L). These results confirm that anti-Scg3 hFab selectively targets Scg3 to ameliorate MCNV and indicate independent roles for Scg3 and VEGF in driving MCNV.

3.8. Minimal Scg3 binding to healthy endothelial and non-endothelial cells

To extend the relative binding repertoires to other cell types known to interact with VEGF, we assessed binding of Scg3-Phage and VEGF-Phage to HUVECs, ARPE19 and Neuron-2a cells. We found low Scg3-specific binding to HUVECs that was partially blocked by anti-Scg3 hFab ($P=0.0248$) or 3C protease cleavage ($P=0.1776$, Figure S7A), and low to insignificant binding to ARPE19 and Neuro-2a cells (Figure S7A). In contrast, we found specific binding of VEGF-Phage to all tested cells that was significantly blocked by excess aflibercept (Figure S7B), consistent with the known functional response of these cells to VEGF (Figure 4) (31, 32). It is noteworthy that HUVECs required Scg3 dosing of 1 μg/ml

to detect functional activity, 10-fold higher than that for VEGF (100 ng/ml) in the *in vitro* functional assay (Figure 4) (10).

4. DISCUSSION

Our recent discovery of Scg3 as a diabetes-selective angiogenic factor raises the possibility that such an activity may extend more broadly to other related neovascular diseases (10). In this regard, the studies reported here provide the following new information: i) In a mouse model of wet AMD, Scg3 binding increase is associated selectively with the developing CNV by at least 6.0-fold relative to healthy choriocapillaris from the same eye (Figure 2E and 9). ii) The absence of co-localization of Scg3 with endothelial marker CD31 suggests that Scg3 promotes CNV by paracrine communication with the CNV vasculature. iii) Markedly reduced CNV severity in $Scg3^{-/-}$ mice confirms a key role of Scg3 in driving pathological angiogenesis in this model. iv) A clinically relevant humanized anti-Scg3 Fab fragment neutralizes CNV with equivalent efficacy to aflibercept. v) *In vitro* studies confirm that Scg3 binding is selective for environments of pathological angiogenesis with low to absent binding to healthy HUVEC, ARPE19 and Neuro-2a cells, each of which displayed positive VEGF binding (Figure S7 and 9). These VEGF-binding cells have been variously implicated in the adverse side effects of anti-VEGF therapy (14, 33, 34).

Previously, by applying the technique of comparative ligandomics, we reported Scg3 binding to DR vessels in diabetic mice with an apparent 1,731-fold increase relative to control mice (1,731:0 for diabetic:healthy) (10). A critical question is whether the 6.0-fold increase in Scg3 binding to CNV found in this study is meaningful when compared to the extremely different results in the DR model. We propose that it is meaningful because the apparent discrepancies in magnitude of the binding can be attributed in part to the radically different methods used for binding quantification. In ligandomics profiling, the high reading of Scg3 binding to DR vessels was arbitrarily exaggerated by PCR amplification of cDNA inserts of enriched vessel-bound phages, including Scg3-displaying phages, for next-generation sequencing (NGS) (10). As a result, NGS-based ligandomics represents a different technical platform from the clonal Scg3-Phage binding assay used in the present study, the latter of which is more closely related to traditional ligand binding assays. The relatively low background binding of Scg3 to healthy vessels in our ligandomics screens can be attributed at least in part to the presence of vast excesses of cDNA library phages that effectively eliminate non-specific binding of Scg3-displaying phage to the target blood vessels. Inclusion of such background phages in the clonal Scg3-Phage binding assay would interfere with phage quantification by plaque assay. As a result, a relatively high background binding of Scg3-Phage to healthy vessels was detected in the present study (Figure 2E), thereby reducing the fold increase of Scg3 binding to CNV vessels. To confirm this speculation, we performed a similar Scg3-Phage binding assay in streptozotocin-induced 4-month-diabetic mice and detected approximately 17.8-fold increase in Scg3 binding to DR vessels (unpublished data). Therefore, we conclude that the 6.0-fold increase in Scg3 binding to CNV vasculature reported here is a more accurate and realistic measurement than the 1,731-fold increase in DR profiled by ligandomics.

Using the new binding assay, we confirmed that Scg3 is a disease-selective endothelial ligand that preferentially binds to CNV vessels over healthy choriocapillaris, whereas VEGF binds to both CNV and healthy choriocapillaris at similar levels (Figure 2E,G). Increased Scg3 binding to diseased vessels is presumed to be conferred by the enhanced availability of an as yet unidentified Scg3R, whereas upregulation of VEGF ligand is the accepted primary driving force for VEGF-mediated pathological angiogenesis (10, 12, 28, 35-37). Such fundamentally distinct mechanisms have profound implications for therapy. While secreted VEGF circulates globally to non-selectively regulate all target cells and vessels that express VEGF receptors, our results indicate that upregulated Scg3 binding appears to be restricted to the surface of diseased endothelia so that Scg3-directed angiogenesis is limited to diseased vasculatures. Therefore, blockade of Scg3 constitutes a novel ligand-guided disease-targeted anti-angiogenic therapy that is predicted to elicit minimal side effects on healthy vasculatures.

It is technically challenging to quantify ligand binding to cultured cells by conventional methods. Indeed, VEGF binding to endothelial VEGFRs required ^{125}I labelling (38). *In vivo* binding with ^{125}I-VEGF is challenging (39), because the VEGF165 homodimer with only 45 kDa is permeable even to healthy vessels (40). Advantages of our new binding assay include the large size of phage articles that are impermeable even to pathological vasculatures, sensitivity to detect single copies of vessel-bound phages by plaque assay, and controllable washing time and conditions to minimize ligand-receptor dissociation. A previous study reported that hyper-permeable vasculatures in pathological conditions are leaky to proteins up to 2,000 kDa (40). T7 phages with diameters of ~55 nm, equivalent to proteins of ≥90,000 kDa (10), are impermeable to all vessels, including CNV. The large phage size is also likely the reason for the failure of intravitreally injected Scg3-Phage to penetrate through the retina and bind to CNV vessels in Fig. S2A. To minimize phage leakage and retain ligand-receptor association, we also optimized perfusion conditions and corroborated the assay by immunohistochemistry (Figures 2H, S1 and S2A) and with multiple controls (Figures 2D,F). We have successfully applied the binding assay to define and compare disease selectivity of Scg3 and VEGF in various angiogenic diseases, including ROP (unpublished data).

When combined with comparative ligandomics, our new ligand binding assay represents a novel approach to discover and validate disease-selective endothelial ligands that have minimal binding and functional activities in healthy vasculature and, therefore, may be overlooked by conventional methods. However, a caveat is that not all ligand proteins can be displayed on phage surfaces with the native motifs necessary for receptor binding due to potential issues of appropriate protein folding, glycosylation and other posttranslational modifications. Therefore, individual ligands displayed on T7 phage should be appropriately tested before application to ligand binding assay, as described in Figure 2A,B.

An apparent anomaly is the negligible Scg3 binding to healthy endothelia *in vivo* vs. significant functional and binding activities on HUVECs (Figure 2E vs. Figures 4 and S7). Previously we noted a similar anomaly as possible results of dose effects (10). Additionally, the *in vitro* binding assays with controllable experimental conditions, including cultured cells with few variations, thorough washing and minimal time for ligand-receptor

dissociation, are likely more sensitive to quantify Scg3 and VEGF binding to HUVECs than the *in vivo* endothelial binding (Figure S7 vs. Figures 2E,G).

Whereas human choroidal endothelial cells (HCECs) represent the preferred substrate for *in vitro* ligand binding assay and hFab characterizations, we found that commercially available HCECs demonstrated low anti-CD31 mAb staining and inconsistent functional phenotypes (data not shown). The retina is supplied by two vascular systems, including retinal and choroidal vasculatures. The former is inside the eye, and its abnormal growth leads to proliferative retinopathy with retinal neovascularization. The latter is outside the eye, and its aberrant growth toward the retina results in CNV. These two vasculatures are considered morphologically and functionally distinct. Instead of choosing HRMVECs, we used the HUVECs as extraocular endothelial cells to substitute HCECs for *in vitro* assays.

The advent of anti-VEGF therapy for wet AMD constitutes a major breakthrough over traditional photodynamic therapy (4). Despite numerous advantages, anti-VEGF therapy has several limitations, including high proportions of patients with limited efficacy and adverse side effects (33, 41, 42). Because of few options, patients that respond poorly to one VEGF inhibitor are often switched to another anti-VEGF regimen despite their similar mechanisms and limited benefits (43). Key factors that may contribute to suboptimal response include: i) the presence of alternative proangiogenic factors that continue to drive pathological angiogenesis and leaky vascular networks even in the presence of optimal VEGF neutralization, and ii) loss of protective functions especially those directed at neurons and RPEs that result from chronic blockade of the VEGF pathway. VEGF is a growth and survival factor not only for endothelial cells but also neurons and RPE cells (Figure S7B and 9) (31, 32). Potential safety concerns of intravitreal anti-VEGF include neurotoxicity and geographic atrophy (33, 41), the latter of which is characterized by the loss of RPE and photoreceptors. Indeed, clinical trials revealed that excessively high doses of ranibizumab inversely reduced long-term visual acuity despite improvements of anatomical retinal structure, such as retinal thickness (44, 45).

It is appropriate to question the mechanisms whereby anti-Scg3 or anti-VEGF can individually inhibit > 50% of CNV (Figure 5A-F). Although Scg3 and VEGF stimulate angiogenesis through distinct receptor pathways (10), all angiogenic pathways converge to induce endothelial proliferation and migration. Therefore, disruption of any signaling pathway that regulates such functions is predicted to block pathological angiogenesis. For example, the chemokine receptor CCR3 was previously reported to be an angiogenic receptor specifically expressed on CNV ECs, and inhibition of CCR3 alone was shown to ameliorate laser-induced CNV by more than 50% (46). However, CCR3 was not upregulated in MCNV, and inhibition of the receptor failed to alleviate MCNV (47). Furthermore, CCR3 is highly expressed on normal eosinophils, and deletion of the CCR3 gene dysregulates the trafficking of eosinophils (48). A Phase 1 clinical trial of a CCR3 antagonist was subjected to early termination (Clinicaltrials.gov #NCT01551771). As a result, anti-Scg3 hFab has the potential to become the first ligand-guided disease-targeted anti-angiogenic therapy.

Because Scg3 and VEGF signal through distinct receptor pathways (10), we predicted and confirmed that the combination of anti-Scg3 and anti-VEGF synergistically ameliorated

MCNV (Figure 7). These results suggest that anti-Scg3 hFab can improve the efficacy of anti-VEGF through alternative or combination therapy.

Because of the stringent disease selectivity of Scg3, we predict that anti-Scg3 hFab provides equivalent efficacy to anti-VEGF but does not affect healthy vessels, RPE or neurons (Figure 9). Thus, anti-Scg3 therapy for DR, wet AMD, ROP and cancer in clinical settings will have optimal safety. Such a safety profile is consistent with the normal phenotype of Scg3-null mice (Figure S6) (30). We found no defect in the development of the vascular and neural systems in $Scg3^{-/-}$ mice. In contrast, mice with the deletion of a single allele of the VEGF gene are embryonic lethal with severely defective vasculogenesis (49).

In conclusion, using a novel phage-based ligand binding assay we describe CNV-selective binding of Scg3 and corresponding disease-restricted angiogenesis (Figure 9). An engineered anti-Scg3 hFab demonstrated high efficacy to alleviate CNV in the context of wet AMD. Anti-Scg3 hFab has disruptive potential to become a unique ligand-guided disease-targeted anti-angiogenic therapy for CNV as sole therapy or combined with anti-VEGF.

Supplementary Material

Refer to Web version on PubMed Central for supplementary material.

ACKNOWLEDGMENTS

We thank Drs. Yingbin Fu, Philp Rosenfeld and Rong Wen for scientific discussion and Dr. Yuqin Wang for technical support. This work was supported by NIH R01EY027749 (WL), R24EY028764 (WL and KAW), R24EY028764-01A1S1 (WL and KAW), R43EY031238 (HT, KAW and WL), R43EY031643 (HT), R43EY032827 (HT and WL), R41EY027665 (WL and HT), American Diabetes Association 1-18-IBS-172 (WL), NIH P30EY002520, P30EY014801, Knights Templar Eye Foundation Endowment in Ophthalmology (WL) and unrestricted institutional grants from Research to Prevent Blindness (RPB) to the Department of Ophthalmology, University of Miami and Department of Ophthalmology, Baylor College of Medicine.

Nonstandard abbreviations:

AF488	Alexa Fluor 488
AMD	age-related macular degeneration
CNV	choroidal neovascularization
DR	diabetic retinopathy
FA	fluorescein angiography
hAb	humanized antibody
hFab	humanized or human antibody Fab fragment
HUVEC	human umbilical vein endothelial cells
IB4	isolectin B4
INL	inner nuclear layer

IPL	inner plexiform layer
mAb	monoclonal antibody
MCNV	Matrigel-induced CNV
OCT	optical coherence tomography
ONL	outer nuclear layer
OPL	outer plexiform layer
RGC	retinal ganglion cell
RPE	retinal pigment epithelium
Scg3	secretogranin III
Scg3R	Scg3 receptor
SIM	structured illumination microscope
VEGF	vascular endothelial growth factor

REFERENCES

1. Wong WL, Su X, Li X, Cheung CMG, Klein R, Cheng C-Y, and Wong TY (2014) Global prevalence of age-related macular degeneration and disease burden projection for 2020 and 2040: a systematic review and meta-analysis. Lancet Glob Health 2, e106–116 [PubMed: 25104651]
2. Baumal CR (2020) Wet age-related macular degeneration: treatment advances to reduce the injection burden. Am J Manag Care 26, S103–S111 [PubMed: 32479026]
3. Shao J, Choudhary MM, and Schachat AP (2016) Neovascular Age-Related Macular Degeneration. Dev Ophthalmol 55, 125–136 [PubMed: 26501146]
4. Brown DM, Michels M, Kaiser PK, Heier JS, Sy JP, Ianchulev T, and ANCHOR Study Group. (2009) Ranibizumab versus verteporfin photodynamic therapy for neovascular age-related macular degeneration: Two-year results of the ANCHOR study. Ophthalmology 116, 57–65.e5 [PubMed: 19118696]
5. Comparison of Age-related Macular Degeneration Treatments Trials (CATT) Research Group, Maguire MG, Martin DF, Ying G-S, Jaffe GJ, Daniel E, Grunwald JE, Toth CA, Ferris FL, and Fine SL (2016) Five-Year Outcomes with Anti-Vascular Endothelial Growth Factor Treatment of Neovascular Age-Related Macular Degeneration: The Comparison of Age-Related Macular Degeneration Treatments Trials. Ophthalmology 123, 1751–1761 [PubMed: 27156698]
6. Mettu PS, Allingham MJ, and Cousins SW (2020) Incomplete response to Anti-VEGF therapy in neovascular AMD: Exploring disease mechanisms and therapeutic opportunities. Prog Retin Eye Res 100906 [PubMed: 33022379]
7. Samanta A, Aziz AA, Jhingan M, Singh SR, Khanani AM, and Chhablani J (2020) Emerging Therapies in Neovascular Age-Related Macular Degeneration in 2020. Asia Pac J Ophthalmol (Phila) 9, 250–259 [PubMed: 32511123]
8. Gonzalez-Buendia L, Delgado-Tirado S, An M, O'Hare M, Amarnani D, A B Whitmore H, Zhao G, Ruiz-Moreno JM, Arboleda-Velasquez JF, and Kim LA (2021) Treatment of Experimental Choroidal Neovascularization via RUNX1 Inhibition. Am J Pathol 191, 418–424 [PubMed: 33345998]
9. Bucher F, Aguilar E, Marra KV, Rapp J, Arnold J, Diaz-Aguilar S, Lange C, Agostini H, Schlunck G, Stahl A, and Friedlander M (2020) CNTF Prevents Development of Outer Retinal Neovascularization Through Upregulation of CxCl10. Invest Ophthalmol Vis Sci 61, 20

10. LeBlanc ME, Wang W, Chen X, Caberoy NB, Guo F, Shen C, Ji Y, Tian H, Wang H, Chen R, and Li W (2017) Secretogranin III as a disease-associated ligand for antiangiogenic therapy of diabetic retinopathy. J Exp Med 214, 1029–1047 [PubMed: 28330905]
11. Rong X, Tian H, Yang L, and Li W (2019) Function-first ligandomics for ocular vascular research and drug target discovery. Exp Eye Res 182, 57–64 [PubMed: 30904565]
12. Li W, Pang I-H, Pacheco MTF, and Tian H (2018) Ligandomics: a paradigm shift in biological drug discovery. Drug Discov Today 23, 636–643 [PubMed: 29326083]
13. LeBlanc ME, Wang W, Ji Y, Tian H, Liu D, Zhang X, and Li W (2019) Secretogranin III as a novel target for the therapy of choroidal neovascularization. Exp Eye Res 181, 120–126 [PubMed: 30633921]
14. Tang F, LeBlanc ME, Wang W, Liang D, Chen P, Chou T-H, Tian H, and Li W (2019) Anti-secretogranin III therapy of oxygen-induced retinopathy with optimal safety. Angiogenesis 22, 369–382 [PubMed: 30644010]
15. Ottiger HP, Battenberg EF, Tsou AP, Bloom FE, and Sutcliffe JG (1990) 1B1075: a brain- and pituitary-specific mRNA that encodes a novel chromogranin/secretogranin-like component of intracellular vesicles. J Neurosci 10, 3135–3147 [PubMed: 2204688]
16. Caberoy NB, Zhou Y, and Li W (2010) Tubby and tubby-like protein 1 are new MerTK ligands for phagocytosis. EMBO J 29, 3898–3910 [PubMed: 20978472]
17. Estep P, Reid F, Nauman C, Liu Y, Sun T, Sun J, and Xu Y (2013) High throughput solution-based measurement of antibody-antigen affinity and epitope binning. MAbs 5, 270–278 [PubMed: 23575269]
18. Cao J, Zhao L, Li Y, Liu Y, Xiao W, Song Y, Luo L, Huang D, Yancopoulos GD, Wiegand SJ, and Wen R (2010) A subretinal matrigel rat choroidal neovascularization (CNV) model and inhibition of CNV and associated inflammation and fibrosis by VEGF trap. Invest Ophthalmol Vis Sci 51, 6009–6017 [PubMed: 20538989]
19. Tang F, Pacheco MTF, Chen P, Liang D, and Li W (2018) Secretogranin III promotes angiogenesis through MEK/ERK signaling pathway. Biochem Biophys Res Commun 495, 781–786 [PubMed: 29154827]
20. Caberoy NB, Zhou Y, Jiang X, Alvarado G, and Li W (2010) Efficient identification of tubby-binding proteins by an improved system of T7 phage display. J Mol Recognit 23, 74–83 [PubMed: 19718693]
21. Wang W, LeBlanc ME, Chen X, Chen P, Ji Y, Brewer M, Tian H, Spring SR, Webster KA, and Li W (2017) Pathogenic role and therapeutic potential of pleiotrophin in mouse models of ocular vascular disease. Angiogenesis 20, 479–492 [PubMed: 28447229]
22. Tokuda K, Baron B, Kuramitsu Y, Kitagawa T, Tokuda N, Morishige N, Kobayashi M, Kimura K, Nakamura K, and Sonoda K-H (2018) Optimization of fixative solution for retinal morphology: a comparison with Davidson's fixative and other fixation solutions. Jpn J Ophthalmol 62, 481–490 [PubMed: 29691783]
23. LeBlanc ME, Wang W, Chen X, Ji Y, Shakya A, Shen C, Zhang C, Gonzalez V, Brewer M, Ma J-X, Wen R, Zhang F, and Li W (2016) The regulatory role of hepatoma-derived growth factor as an angiogenic factor in the eye. Mol Vis 22, 374–386 [PubMed: 27122967]
24. Li W, Webster KA, LeBlanc ME, and Tian H (2018) Secretogranin III: a diabetic retinopathy-selective angiogenic factor. Cell Mol Life Sci 75, 635–647 [PubMed: 28856381]
25. Hosaka M and Watanabe T (2010) Secretogranin III: a bridge between core hormone aggregates and the secretory granule membrane. Endocr J 57, 275–286 [PubMed: 20203425]
26. LeBlanc ME, Wang W, Caberoy NB, Chen X, Guo F, Alvarado G, Shen C, Wang F, Wang H, Chen R, Liu Z-J, Webster K, and Li W (2015) Hepatoma-derived growth factor-related protein-3 is a novel angiogenic factor. PLoS One 10, e0127904 [PubMed: 25996149]
27. Ji L, Tian H, Webster KA, and Li W (2021) Neurovascular regulation in diabetic retinopathy and emerging therapies. Cell Mol Life Sci 78, 5977–5985 [PubMed: 34230991]
28. Hara C, Kasai A, Gomi F, Satooka T, Sakimoto S, Nakai K, Yoshioka Y, Yamamuro A, Maeda S, and Nishida K (2013) Laser-induced choroidal neovascularization in mice attenuated by deficiency in the apelin-APJ system. Invest Ophthalmol Vis Sci 54, 4321–4329 [PubMed: 23722395]

29. Abhinandan KR and Martin ACR (2007) Analyzing the “degree of humanness” of antibody sequences. J Mol Biol 369, 852–862 [PubMed: 17442342]
30. Kingsley DM, Rinchik EM, Russell LB, Ottiger HP, Sutcliffe JG, Copeland NG, and Jenkins NA (1990) Genetic ablation of a mouse gene expressed specifically in brain. EMBO J 9, 395–399 [PubMed: 2303033]
31. Calvo PM, Pastor AM, and de la Cruz RR (2018) Vascular endothelial growth factor: an essential neurotrophic factor for motoneurons? Neural Regen Res 13, 1181–1182 [PubMed: 30028320]
32. Byeon SH, Lee SC, Choi SH, Lee H-K, Lee JH, Chu YK, and Kwon OW (2010) Vascular endothelial growth factor as an autocrine survival factor for retinal pigment epithelial cells under oxidative stress via the VEGF-R2/PI3K/Akt. Invest Ophthalmol Vis Sci 51, 1190–1197 [PubMed: 19834034]
33. Grunwald JE, Pistilli M, Daniel E, Ying G-S, Pan W, Jaffe GJ, Toth CA, Hagstrom SA, Maguire MG, Martin DF, and Comparison of Age-Related Macular Degeneration Treatments Trials Research Group. (2017) Incidence and Growth of Geographic Atrophy during 5 Years of Comparison of Age-Related Macular Degeneration Treatments Trials. Ophthalmology 124, 97–104 [PubMed: 28079023]
34. Morin J, Luu TM, Superstein R, Ospina LH, Lefebvre F, Simard M-N, Shah V, Shah PS, Kelly EN, and Canadian Neonatal Network and the Canadian Neonatal Follow-Up Network Investigators. (2016) Neurodevelopmental Outcomes Following Bevacizumab Injections for Retinopathy of Prematurity. Pediatrics 137
35. Aiello LP, Avery RL, Arrigg PG, Keyt BA, Jampel HD, Shah ST, Pasquale LR, Thieme H, Iwamoto MA, and Park JE (1994) Vascular endothelial growth factor in ocular fluid of patients with diabetic retinopathy and other retinal disorders. N Engl J Med 331, 1480–1487 [PubMed: 7526212]
36. Watanabe D, Suzuma K, Matsui S, Kurimoto M, Kiryu J, Kita M, Suzuma I, Ohashi H, Ojima T, Murakami T, Kobayashi T, Masuda S, Nagao M, Yoshimura N, and Takagi H (2005) Erythropoietin as a retinal angiogenic factor in proliferative diabetic retinopathy. N Engl J Med 353, 782–792 [PubMed: 16120858]
37. Matsunaga N, Chikaraishi Y, Izuta H, Ogata N, Shimazawa M, Matsumura M, and Hara H (2008) Role of soluble vascular endothelial growth factor receptor-1 in the vitreous in proliferative diabetic retinopathy. Ophthalmology 115, 1916–1922 [PubMed: 18718666]
38. Gitay-Goren H, Cohen T, Tessler S, Soker S, Gengrinovitch S, Rockwell P, Klagsbrun M, Levi BZ, and Neufeld G (1996) Selective binding of VEGF121 to one of the three vascular endothelial growth factor receptors of vascular endothelial cells. J Biol Chem 271, 5519–5523 [PubMed: 8621410]
39. Cooper ME, Vranes D, Youssef S, Stacker SA, Cox AJ, Rizkalla B, Casley DJ, Bach LA, Kelly DJ, and Gilbert RE (1999) Increased renal expression of vascular endothelial growth factor (VEGF) and its receptor VEGFR-2 in experimental diabetes. Diabetes 48, 2229–2239 [PubMed: 10535459]
40. Egawa G, Nakamizo S, Natsuaki Y, Doi H, Miyachi Y, and Kabashima K (2013) Intravital analysis of vascular permeability in mice using two-photon microscopy. Sci Rep 3, 1932 [PubMed: 23732999]
41. Sultana J, Scondotto G, Cutroneo PM, Morgante F, and Trifirò G (2020) Intravitreal Anti-VEGF Drugs and Signals of Dementia and Parkinson-Like Events: Analysis of the VigiBase Database of Spontaneous Reports. Front Pharmacol 11, 315 [PubMed: 32226387]
42. Dedania VS and Bakri SJ (2015) Current perspectives on ranibizumab. Clin Ophthalmol 9, 533–542 [PubMed: 25848203]
43. Pinheiro-Costa J, Costa JM, Beato JN, Freitas-da-Costa P, Brandão E, Falcão MS, Falcão-Reis F, and Carneiro ÂM (2015) Switch to Aflibercept in the Treatment of Neovascular AMD: One-Year Results in Clinical Practice. Ophthalmologica 233, 155–161 [PubMed: 25896317]
44. Sepah YJ, Sadiq MA, Boyer D, Callanan D, Gallemore R, Bennett M, Marcus D, Halperin L, Hassan M, Campochiaro PA, Nguyen QD, Do DV, and READ-3 Study Group. (2016) Twenty-four-Month Outcomes of the Ranibizumab for Edema of the Macula in Diabetes - Protocol 3 with High Dose (READ-3) Study. Ophthalmology 123, 2581–2587 [PubMed: 27707550]

45. Ho AC, Busbee BG, Regillo CD, Wieland MR, Van Everen SA, Li Z, Rubio RG, Lai P, and HARBOR Study Group. (2014) Twenty-four-month efficacy and safety of 0.5 mg or 2.0 mg ranibizumab in patients with subfoveal neovascular age-related macular degeneration. Ophthalmology 121, 2181–2192 [PubMed: 25015215]

46. Takeda A, Baffi JZ, Kleinman ME, Cho WG, Nozaki M, Yamada K, Kaneko H, Albuquerque RJC, Dridi S, Saito K, Raisler BJ, Budd SJ, Geisen P, Munitz A, Ambati BK, Green MG, Ishibashi T, Wright JD, Humbles AA, Gerard CJ, Ogura Y, Pan Y, Smith JR, Grisanti S, Hartnett ME, Rothenberg ME, and Ambati J (2009) CCR3 is a target for age-related macular degeneration diagnosis and therapy. Nature 460, 225–230 [PubMed: 19525930]

47. Li Y, Huang D, Xia X, Wang Z, Luo L, and Wen R (2011) CCR3 and choroidal neovascularization. PLoS One 6, e17106 [PubMed: 21358803]

48. Humbles AA, Lu B, Friend DS, Okinaga S, Lora J, Al-Garawi A, Martin TR, Gerard NP, and Gerard C (2002) The murine CCR3 receptor regulates both the role of eosinophils and mast cells in allergen-induced airway inflammation and hyperresponsiveness. Proc Natl Acad Sci U S A 99, 1479–1484 [PubMed: 11830666]

49. Ferrara N, Carver-Moore K, Chen H, Dowd M, Lu L, O'Shea KS, Powell-Braxton L, Hillan KJ, and Moore MW (1996) Heterozygous embryonic lethality induced by targeted inactivation of the VEGF gene. Nature 380, 439–442 [PubMed: 8602242]

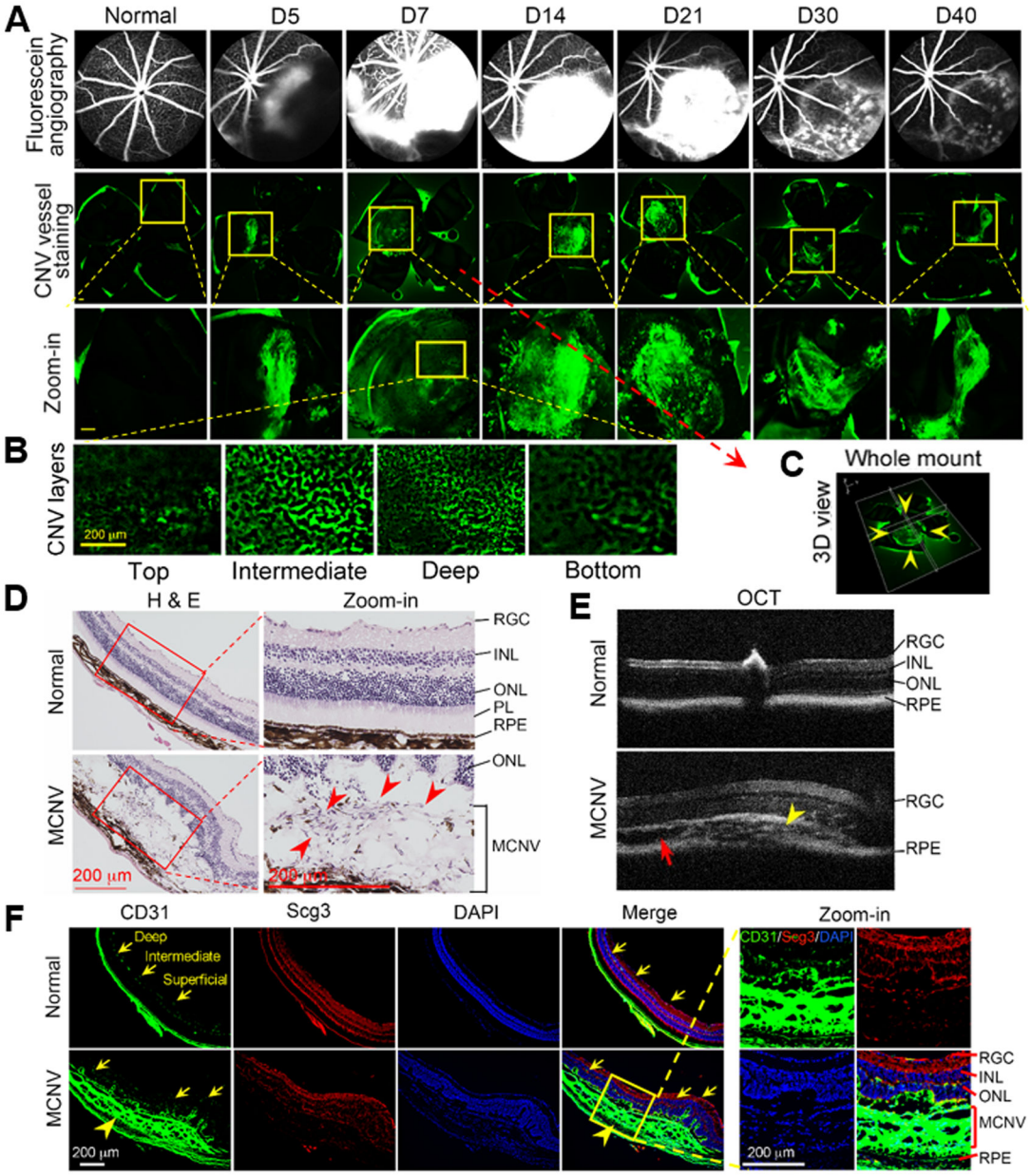

Figure 1. Longitudinal evolution of MCNV.

(A) Representative FA images (upper panel) or CNV vessel staining (middle and bottom panels) at indicated days post subretinal injection of Matrigel. **(B)** Different layers of CNV vessels, including top, intermediate, deep and bottom layer. **(C)** 3D view of the CNV at Day 7 (middle row in Panel A). Arrowheads indicate CNV. **(D)** H&E staining of the retina and choroid of normal and MCNV mice on Day 7 post CNV induction. **(E)** OCT retinal images of normal and MCNV mice on Day 7. Arrowheads in D and E indicate CNV lesion, and arrow in E indicates retinal detachment. **(F)** Immunohistochemistry to detect the retinal expression of Scg3 and CD31 in healthy and MCNV mice on Day 7. Arrows indicate superficial, intermediate and deep retinal vascular plexuses in the inner retina, whereas arrowhead shows Matrigel with ingrown CNV vessels. RGC, retinal ganglion cell; INL,

inner nuclear layer; OPL, outer plexiform layer; ONL, outer nuclear layer; RPE, retinal pigment epithelium. Scale = 200 μm.

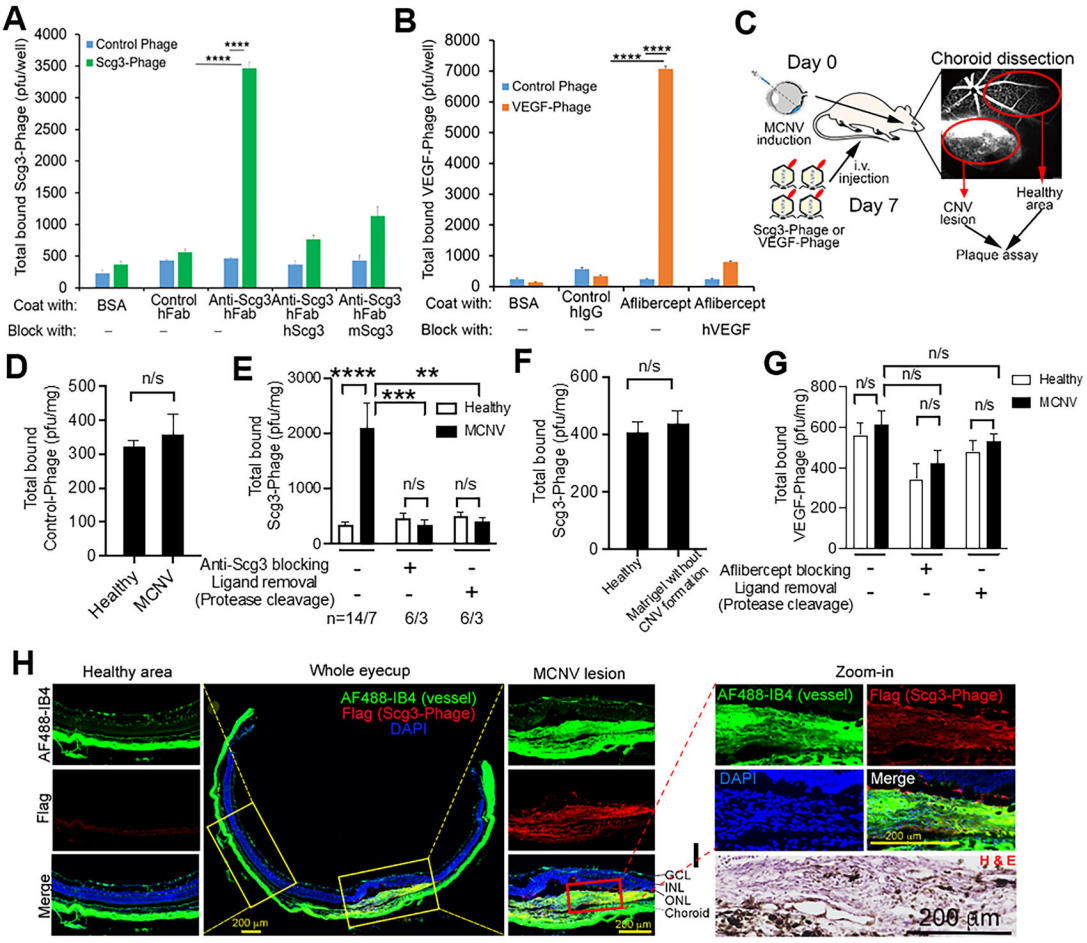

Figure 2. Scg3 selectively binds CNV vessels.

(A) *In vitro* binding of Scg3-Phage to immobilized anti-Scg3 hFab on ELISA plates in the presence or absence of excess hScg3 of mScg3. n = 3 wells/group. **(B)** *In vitro* binding of VEGF-Phage to immobilized aflibercept with or without excess VEGF blocking. n = 3 wells/group. **(C)** Schematic of *in vivo* ligand binding assay in D-G. Scg3-Phage, VEGF-Phage or control phage was injected i.v. to quantify ligand binding in MCNV vessels and healthy choriocapillaris. Choroids with or without CNV lesion were dissected from the same eye to quantify vessel-bound phages. **(D)** Quantification of vessel-bound control phage in choroids with or without CNV lesion. n=6 eyes in 3 mice/group. **(E)** Quantification of vessel-bound Scg3-Phage in choroids with or without CNV lesion. Scg3-Phage was pre-incubated with or without HRV 3C protease to cleave and remove Scg3 from the phage surface and pre-incubated with or without anti-Scg3 hFab before i.v. injection for *in vivo* ligand binding assay. n (# eyes/# mice per group) is indicated at the bottom of the graph. **(F)** Quantification of vessel-bound Scg3-phage in choroids with or without Matrigel, which was injected 1 h before the binding assay without CNV formation. n=10 eyes in 5 mice/group. **(G)** Quantification of vessel-bound VEGF-Phage in choroids with or without CNV and the pretreatment of aflibercept or 3C protease. n=6 eyes in 3 mice/group. **(H)** Visualization of *in vivo* ligand binding using anti-Flag mAb to detect vessel-bound FLAG-tagged Scg3-Phage and AF488-IB4 to label vessels. **(I)** H&E staining of the retinal section adjacent to Figure

2H. Scale = 200 μm. All CNV at Day 7. ±SEM; * $p<0.05$, **** $p<0.0001$; n/s, not significant; t-test.

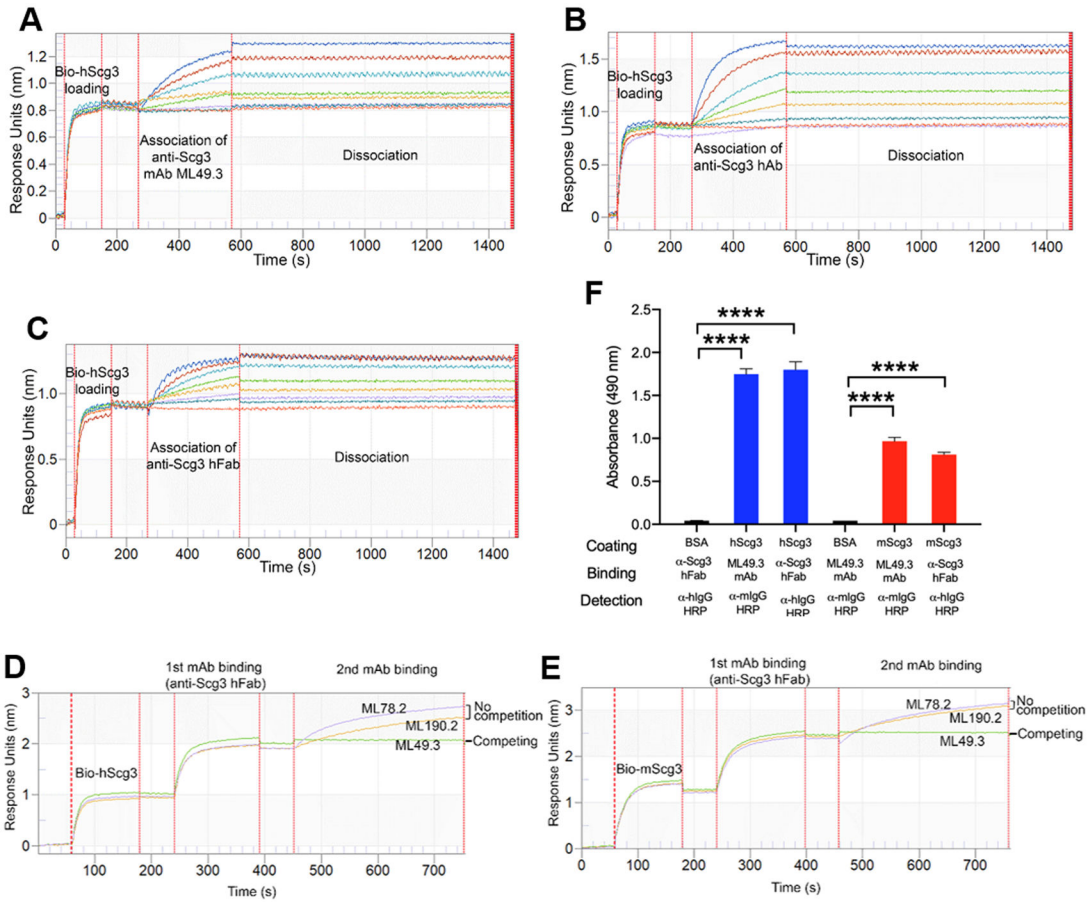

Figure 3. Binding properties of anti-Scg3 mAb, hAb and hFab.

(A-C) Binding kinetics of anti-Scg3 ML49.3 mAb, EBP2 hAb and hFab analyzed by Octet instrument to calculate K_D. **(A)** anti-Scg3 mAb. **(B)** anti-Scg3 hAb. **(C)** anti-Scg3 hFab. **(D, E)** Epitope binning by Octet using biotin-hScg3 **(D)** or biotin-mScg3 **(E)**. Prior binding of anti-Scg3 hFab to Scg3 blocked subsequent binding of ML49.3 mAb, but not ML78.2 and 190.2 mAbs as non-competing controls. **(F)** Ab binding to hScg3 and mScg3 on ELISA plates. n=3 wells/group. ± SEM, **** P<0.0001. t-test.

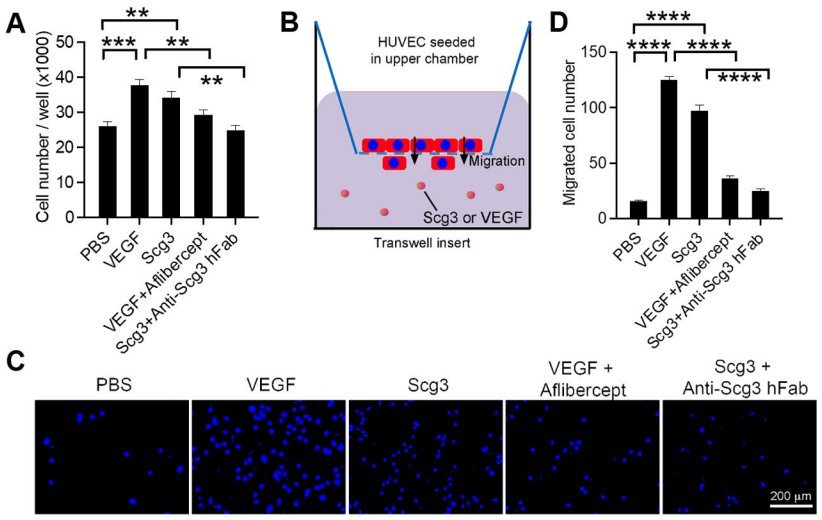

Figure 4. Neutralizing activity of anti-Scg3 hFab.

(A) Anti-Scg3 hFab inhibits Scg3-induced proliferation of HUVECs. Cells were treated with VEGF (100 ng/ml) or Scg3 (1 μg/ml) in the presence or absence of aflibercept (1.5 μg/ml) or anti-Scg3 hFab (2.5 μg/ml), respectively. n = 6 wells/group. **(B)** Illustration of transwell migration assay. HUVECs were seeded in the upper chamber of transwell inserts. Scg3, VEGF or PBS was added to the bottom chamber in the presence or absence of aflibercept or anti-Scg3 hFab (concentrations as in A). Cells migrated through the transwell membrane to the opposite side of the membrane were stained with DAPI and counted, whereas cells on the upper side of the membrane were removed. **(C)** Representative image of migrated cells. Scale = 200 μm. **(D)** Quantification of migrated cells. ±SEM; n = 6 wells/group. ** $p<0.01$, *** $p<0.001$, **** $p<0.0001$; one-way ANOVA test.

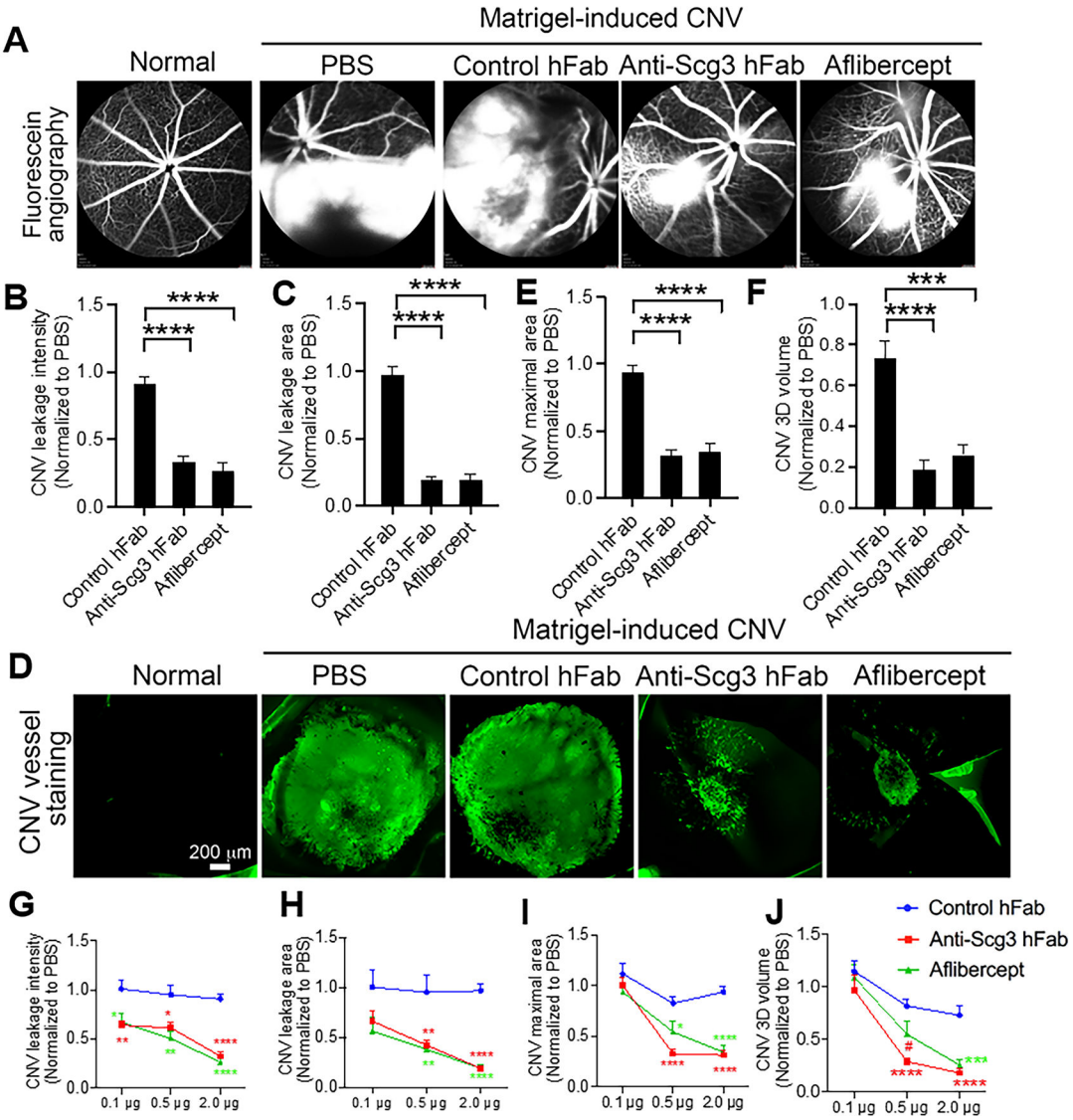

Figure 5. Anti-Scg3 hFab alleviates MCNV.

Mice were intravitreally treated with anti-Scg3 hFab, aflibercept, control hFab (2 μg/1 μl/eye) at Day 3 and analyzed at Day 7 post CNV induction for FA and CNV vessel staining. **(A)** Representative FA images. **(B)** Quantification of relative CNV leakage intensity in A. **(C)** Quantification of CNV leakage area in A. n=7 eyes in 7 mice/group for B and C. **(D)** Representative images of CNV vessel staining using AF488-IB4. **(E)** Quantification of CNV maximal lesion area in D. **(F)** Quantification of CNV 3D volume in D. n=9 eyes in 9 mice/group for E and F. Scale = 200 μm. **(G-J)** Dose-response curve of anti-Scg3 hFab, aflibercept and control hFab (see Figures S3 and S4 for 0.5 and 0.1 μg/eye groups and sample sizes). **(G)** CNV leakage intensity. **(H)** CNV leakage area. **(I)** Maximal area of CNV vessels staining. **(J)** 3D volume of CNV vessels. Data were normalized to PBS treatment. ±SEM. * $p<0.05$; ** $p<0.01$, *** $p<0.001$, **** $P<0.0001$. For G-J, all vs. control hFab except # ($p<0.05$, anti-Scg3 vs. aflibercept). One-way ANOVA test.

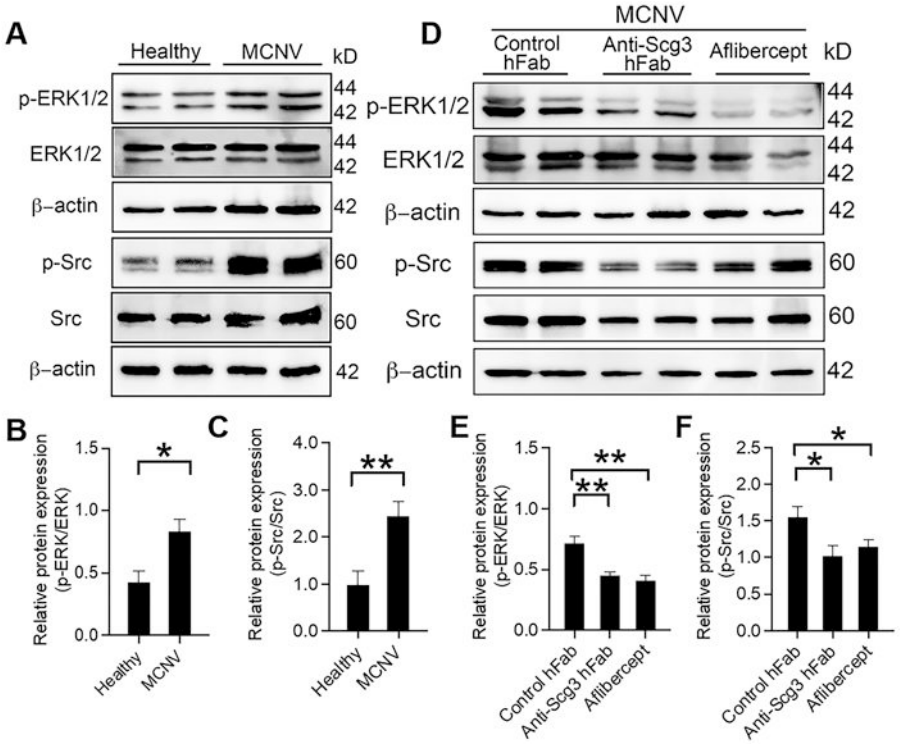

Figure 6. Anti-Scg3 hFab inhibits Scg3-induced phosphorylation of ERK and Src kinases.

(A) Western blotting of phospho-ERK (p-ERK), ERK, p-Src and Src in RPE eyecups (i.e., retina-choroid-sclera complex) isolated from healthy and MCNV mice. **(B)** Quantification of relative band intensity for p-ERK vs. total ERK in A. **(C)** Quantification of p-Src vs. total Src in A. **(D)** Western blotting of p-ERK, ERK, p-Src, Src, and β-actin in RPE eyecups isolated from MCNV mice treated with intravitreal anti-Scg3 hFab, aflibercept or control hFab (2 μg/1 μl/eye). **(E)** Quantification of p-ERK vs. total ERK in D. **(F)** Quantification of p-Src vs. total Src in D. ±SEM. n=6 eyes in 6 mice/group. * $p<0.05$, ** $p<0.01$; one-way ANOVA.

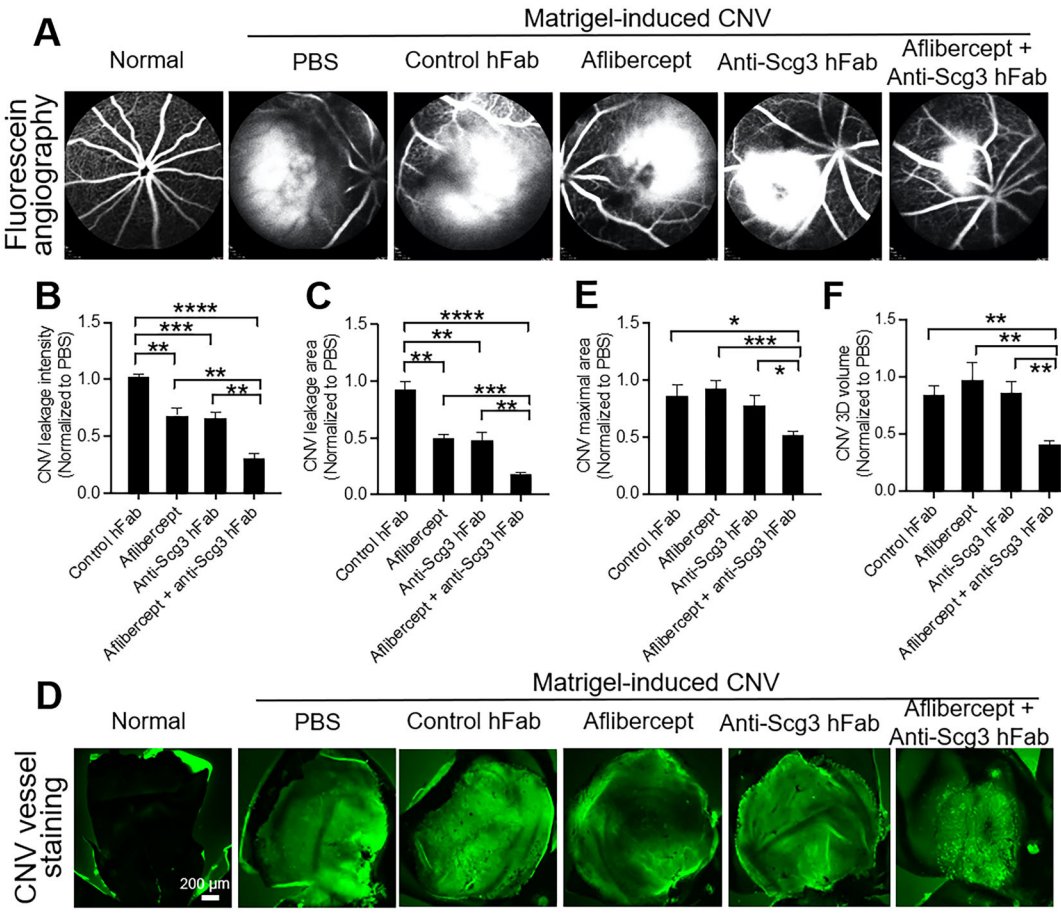

Figure 7. Synergistic combination therapy of anti-Scg3 hFab and aflibercept to alleviate MCNV.

Mice were intravitreally treated with anti-Scg3 hFab, aflibercept, control hFab (0.2 μg/1 μl/eye) or mixture of anti-Scg3 hFab and aflibercept (0.1 + 0.1 μg, 1 μl/eye) at 3 days post MCNV induction and analyzed, as described in Figure 5. **(A)** Representative FA images. **(B)** Quantification of CNV leakage intensity in A. **(C)** Quantification of CNV leakage area in A. n=5 eyes in 5 mice/group for B and C (except 4 eyes in 4 mice for aflibercept). **(D)** Representative images of CNV vessel staining using AF488-IB4. **(E)** Quantification of CNV maximal lesion area in D. **(F)** Quantification of CNV 3D volume in D. n=5 eyes in 5 mice/group for E and F. Scale = 200 μm. Data were normalized to PBS treatment. ±SEM. * p<0.05; ** p<0.01, *** p<0.001, **** P<0.0001. One-way ANOVA test.

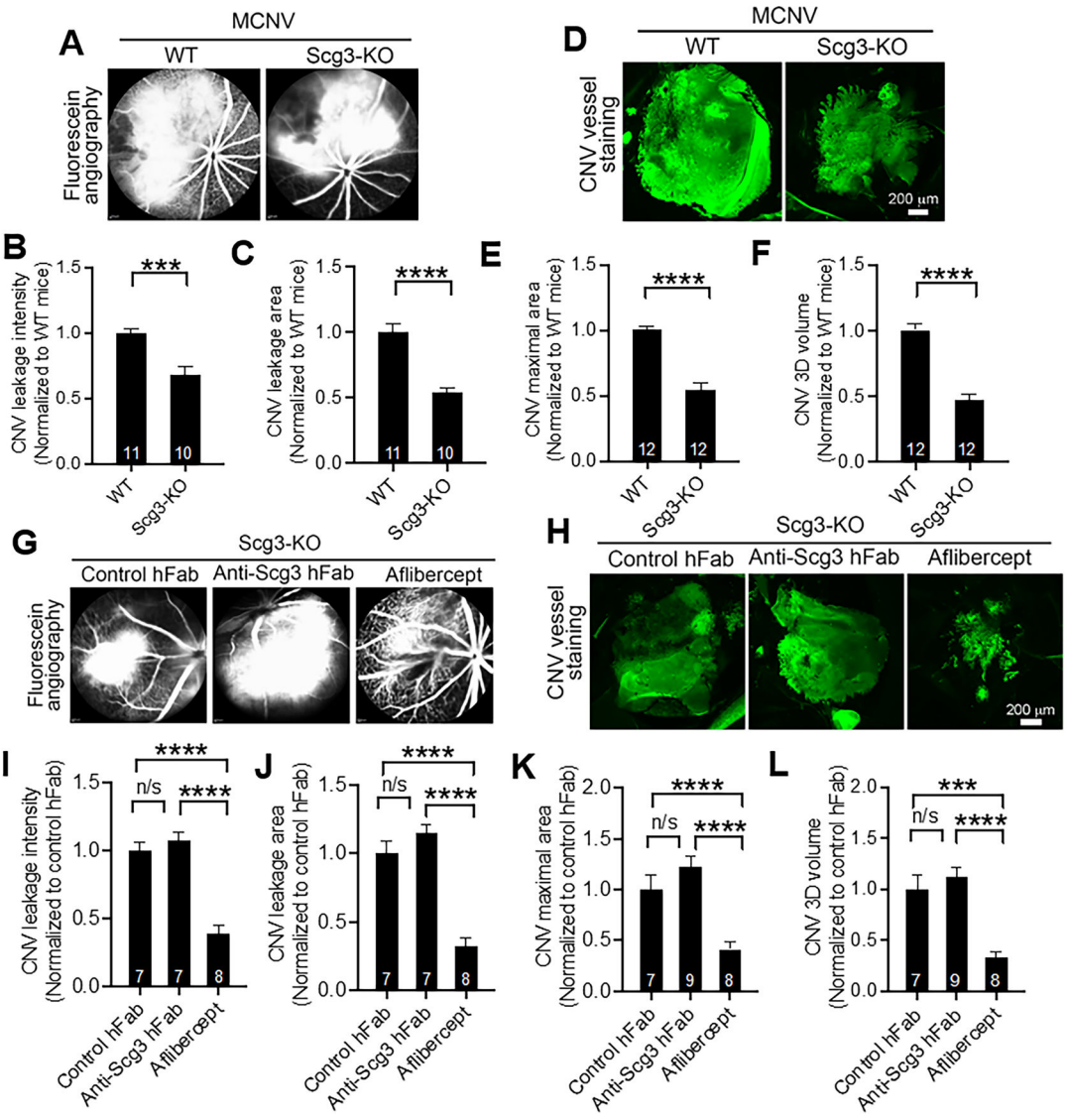

Figure 8. CNV severity and anti-Scg3 therapy in Scg3-deficient mice.

(A-F) MCNV severity in Scg3$^{-/-}$ and Scg3$^{+/+}$ mice. **(A)** Representative FA images of MCNV. **(B)** Quantification of CNV leakage intensity in A. **(C)** Quantification of CNV leakage area size in A. **(D)** Representative image of CNV vessel staining with AF488-IB4. **(E)** Quantification of CNV maximal lesion area in D. **(F)** Quantification of CNV 3D volume in D. **(G-L)** Therapeutic efficacy of anti-Scg3 hFab or aflibercept in Scg3-null mice with MCNV. The description of these panels is similar to A-F but in mice treated with indicated agents (2 μg/1 μl/eye), as described in Figure 5. n (# of eye/group) is indicated inside graphs. All analyses at Day 7 post CNV induction. ±*** SEM; ***p<0.001, **** p<0.0001, n/s, not significant; one-way ANOVA test.

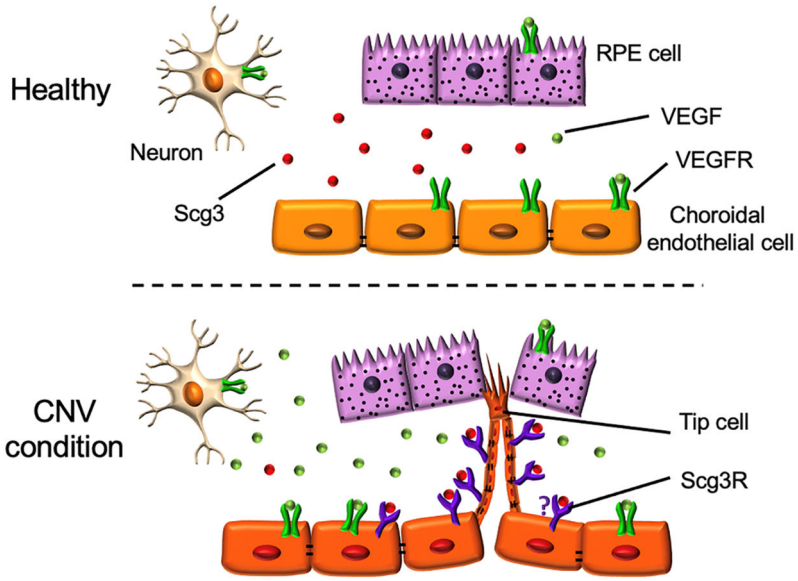

Figure 9.

Summary of disease-selective Scg3 and anti-Scg3 therapy. Scg3 binding to CNV vessels (i.e., Scg3 receptor expression) is markedly upregulated, whereas Scg3 level is minimally increased in CNV. In contrast to increased VEGF expression in CNV, VEGF binding is minimally increased. Unlike VEGF, Scg3 does not bind to healthy endothelial cells, neurons or RPE. Therefore, anti-Scg3 hAb selectively targets CNV vessels with minimal side effects on other cells, whereas anti-VEGF not only inhibits CNV but also exerts adverse side effects on healthy vessels, neurons and RPE.